Measurement and Modeling of Iron Losses in Electrical Machines

Andreas Krings, Shafigh Nategh, Alexander Stening, Henrik Grop, Oskar Wallmark, Juliette Soulard
Laboratory of Electrical Energy Conversion (E2C), Royal Institute of Technology (KTH)
Teknikringen 33
SE-100 44 Stockholm, Sweden
Email: {andreas.krings, shafigh.nategh, alexander.stening, henrik.grop, oskar.wallmark, juliette.soulard}@ee.kth.se

Summary

This paper gives an overview of nowadays used simulation models and measurement methods in order to determine iron losses in electrical machinery. The paper provides machine designers and system engineers with an overview of suitable iron loss models applicable for the machine design process and simulations. Furthermore, possible methods for iron loss measurements in electrical machines are presented from ongoing research projects. Besides standard electrical power measurements, iron losses are determined by thermal and magnetic property measurements, taking into account different IEC and IEEE standards. The goal is to emphasize the different possibilities of iron loss measurement methods and possible application areas for electrical machinery.

1 Introduction

Iron losses in electrical machines have been a concern for decades. They are one of the key points when it comes to efficiency optimization and the development of future high power density machines. But even if electrical machines and iron losses have been studied for more than 100 years, there is still a discrepancy between simulated and measured iron losses in electrical machines. So called "loss correction factors", "machine factors" or "build factors" are used to match the simulations to the corresponding measurement results. These factors are often as large as 2 or even higher, which means that errors between the simulation and measurement results of more than 100% are not uncommon.
The first part of this paper gives a short overview about iron loss models used in the machine design and manufacturing process nowadays. The largest problem for these models is the material parameter identification of the iron sheets. They can change significantly during the manufacturing process of the machine [1,2]. Especially the cutting and punching

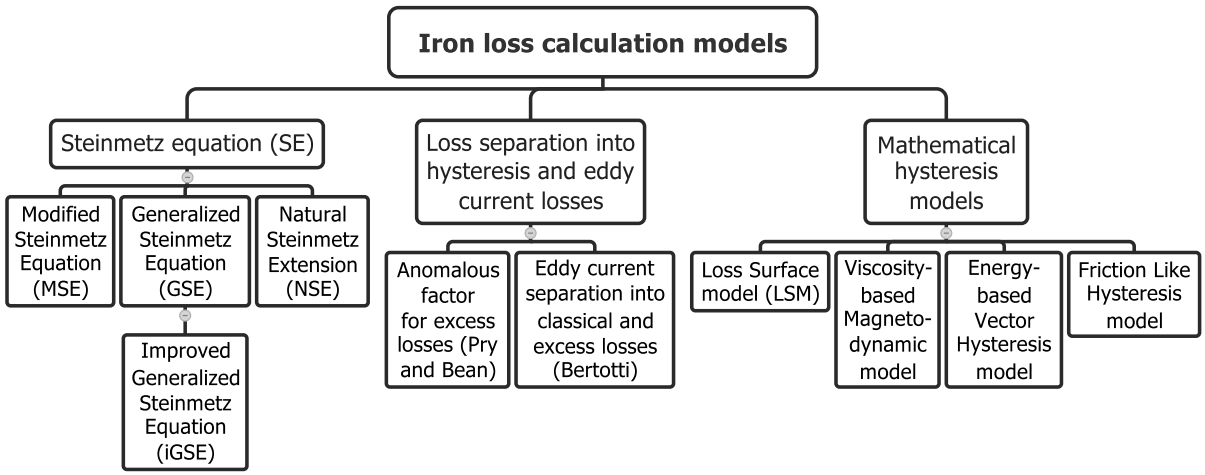

Figure 1: Model approaches to determine iron losses in electrical machines.

processes influence the material properties and create inhomogeneous stresses inside the sheets. The effect is depending on the alloy composite, whereas the grain size in the sheets seems to be the main influencing factor, especially for operating ranges between $0.4\,\mathrm{T}$ to $1.5\,\mathrm{T}$ [3, 4]. Similar deteriorations due to the cutting and punching effect are obtained by the stacking and welding process during the machine core assembly. Especially the welding process deteriorates the material properties of the assembled core which, in turn, generates higher iron losses [5].

The second part focuses on methods to measure and investigate iron losses in different kinds of electrical machines. The iron losses in an induction machine are determined by a loss separation approach based on the total losses measured at no-load. Another iron loss determination approach is to investigate the iron losses by local thermal measurements in conjunction with previously determined thermal models. This approach is validated with a permanent magnet assisted synchronous reluctance machine (PMaSRM). Afterwards, iron loss measurement methods are presented, where the losses are determined by magnetic material investigations and electrical power measurements. These measurements are done on the stator core of small high speed slot-less permanent magnet machines. The same method is used for ring core test specimen made of construction steel to investigate iron losses in passive structure parts of large synchronous generators. Finally, for the same machine a core flux test method is presented to detect iron loss hot spots in the stator yoke by thermal measurements.

2 Iron Loss Models - Overview

A plethora of different iron loss simulation models are used nowadays, from simple empirical Steinmetz equation models to the Preisach and/or Jiles-Atherton and even more complex multidimensional vector based models [6]. Figure 1 gives an overview of several methods which are used for determining iron losses in electrical machines. It should be noted that this overview is not intended to be exhaustive.

2.1 Steinmetz based models

The first group of models is based on the Steinmetz Equation (SE) [7]

$$p_{\mathrm{Fe}} \;=\; C_{\mathrm{SE}}\, f^{\alpha}\, \hat{B}^{\beta} \tag{1}$$

where $\hat{B}$ is the peak value of the flux density in the device under test. The three coefficients C_{SE}, α and β are determined by fitting the loss model to curves from measurement data. Eq. (1) assumes a purely sinusoidal flux density.
A modification of the Steinmetz equation is the *Generalized Steinmetz Equation* (GSE) [8]. It is based on the idea that the instantaneous iron loss is a single-valued function of the flux density B and the rate of change of the flux density dB/dt. A formula is derived which uses this single-valued function and connects it to the Steinmetz coefficients, according to (2).

$$p_{\mathrm{Fe}} \;=\; \frac{1}{T}\int_0^T C_{\mathrm{SE}} \left|\frac{\mathrm{d}B}{\mathrm{d}t}\right|^{\alpha} |B(t)|^{\beta-\alpha}\,\mathrm{d}t \tag{2}$$

An advantage is that the GSE has a DC-bias sensitivity. A disadvantage of the GSE is the accuracy limitation if the third or another relatively low-ordered harmonic of the flux density becomes significant, i.e. if multiple peaks are occurring in the flux density waveform.
To overcome this problem, the GSE was upgraded to the *improved Generalized Steinmetz Equation* (iGSE) [9]. The iGSE splits the waveform in one major and one or more minor loops and thus takes sub loops of the full hysteresis loop into account. This is achieved by a recursive algorithm which calculates the iron losses for each loop separately by

$$p_{\mathrm{Fe_x}} \;=\; \frac{1}{T}\int_0^T C_{\mathrm{SE}} \left|\frac{\mathrm{d}B}{\mathrm{d}t}\right|^{\alpha} |\Delta B|^{\beta-\alpha}\,\mathrm{d}t \tag{3}$$

where ΔB is the peak-to-peak flux density of the current major or minor loop of the waveform.
It should be pointed out that all modifications of the Steinmetz equation have the well known problem that the Steinmetz coefficients vary with frequency. Thus, for waveforms with a high harmonic content, it can be difficult to find applicable coefficients which give good results over the full frequency range of the applied waveform.

2.2 Iron loss separation models

Another approach is to separate the iron losses based on the Steinmetz Equation (1) into static hysteresis losses and dynamic eddy current losses [10]:

$$p_{\mathrm{Fe}} = p_{\mathrm{hyst}} + p_{\mathrm{ec}} = C_{\mathrm{hyst}}\, f\, \hat{B}^2 + C_{\mathrm{ec}}\, f^2\, \hat{B}^2 \tag{4}$$

with C_{hyst} and C_{ec} the hysteresis loss coefficient and the eddy current loss coefficient, respectively. It is assumed that the hysteresis losses are proportional to the hysteresis loop area of the material at low frequencies ($f \to 0\,\mathrm{Hz}$). The eddy current part of the losses p_{ec} can be derived from Maxwell's equations:

$$p_{\mathrm{ec}} = \frac{d^2 \left(\frac{\mathrm{d}B(t)}{\mathrm{d}t}\right)^2}{12\,\rho\,\gamma} \tag{5}$$

where $B(t)$ is the flux density as a function of time, d is the thickness of the electric sheet, ρ its specific resistivity and γ the material density.
Equation (4) has been proven correct for several Nickel-Iron (NiFe) alloys but lacks accuracy for SiFe alloys [11]. For this reason, an empirical correction factor η_{exc}, called the excess loss factor or anomalous loss factor, was introduced [12]. It extends (4) to

$$p_{\mathrm{Fe}} = p_{\mathrm{hyst}} + \eta_{\mathrm{a}}\, p_{\mathrm{ec}} = C_{\mathrm{hyst}}\, f\, \hat{B}^2 + \eta_{\mathrm{exc}}\, C_{\mathrm{ec}}\, f^2\, \hat{B}^2 \tag{6}$$

with $\eta_{\mathrm{exc}} = p_{\mathrm{ec\_measured}}/p_{\mathrm{ec\_calculated}} > 1$. For thin grain oriented SiFe alloys, η_{exc} reaches values between 2 and 3 [11].
In another approach, the excess losses, as a function of the flux density and frequency, are taken into account by adding an additional loss term p_{exc} in (4). Thus, the iron loss formula p_{Fe} is separated into three factors, the static hysteresis losses p_{hyst}, dynamic eddy current losses p_{ec} and the excess losses p_{exc}:

$$p_{\mathrm{Fe}} = p_{\mathrm{hyst}} + p_{\mathrm{ec}} + p_{\mathrm{exc}} = C_{\mathrm{hyst}}\, f\, \hat{B}^2 + C_{\mathrm{ec}}\, f^2\, \hat{B}^2 + C_{\mathrm{exc}}\, f^{1.5}\, \hat{B}^{1.5} \tag{7}$$

where C_{exc} is the excess loss coefficient.
The excess losses in (7) are still based on empirical factors from curve fitting. But a theory and statistical model to determine C_{exc} mathematically is presented in [13,14]. In this model, the excess loss part is described by a physical function in terms of the active magnetic objects and the domain wall motion (Bertotti's statistical model):

$$C_{\mathrm{exc}} = \sqrt{S\, V_0\, \sigma\, G} \tag{8}$$

where S is the cross sectional area of the lamination sample, $G \approx 0.136$ a dimensionless coefficient of the eddy current damping and σ the electric conductivity of the lamination. The factor V_0 characterizes the statistical distribution of the local coercive fields and takes into account the grain size [15]. It has to be noted that this loss separation does not hold if the skin effect is not negligible [16]. A recent study on the properties of the coefficients is presented in [17].
In electrical machines, the iron losses in the tooth tips and in the intersection areas between the teeth and the yoke are mainly caused by rotational flux densities. In the previous mentioned loss models, iron losses due to rotational flux densities are not taken into account. However, there are several approaches investigating this phenomena [18–22]. The iron losses are separated by their magnetizing processes. This means that the losses caused by linear magnetization, rotational magnetization and higher harmonics are added up to determine the total iron losses [23]:

$$p_{\mathrm{Fe}} = C_1\, p_{\mathrm{a}} + C_2\, p_{\mathrm{rot}} + C_3\, p_{\mathrm{hf}} \tag{9}$$

where p_{a} are the losses caused by linear magnetization, p_{rot} the losses caused by rotational magnetization and p_{hf} the losses caused by higher harmonics. C_x are empirical material and geometric dependent factors determined by measurements and curve fittings.
In the middle of the teeth and in the middle of the yoke, the magnetization is linear only. It is therefore depending on the machine geometry if the rotational losses account for a significant part of the total iron losses and if the separation model by the magnetization process can give better results.

A quite new approach to combine the loss separation model (7) with the rotational loss separation model is presented by introducing a rotational loss factor due to rotational magnetization in the former equation [24]:

$$p_{\mathrm{Fe}} = a_2\,\hat{B}^2\,f + (a_1 + a_4\,\hat{B}^{a_3})\hat{B}^2\,f^2 \tag{10}$$

where $a_1 = C_{\mathrm{ec}}$ and $a_2 = C_{\mathrm{hyst}}(1 + (r-1)(B_{\mathrm{min}}/B_{\mathrm{max}}))$, with r the rotational hysteresis factor and B_{min} and B_{max} the minimum and maximum values of $B(t)$ over one period. The factor a_4 and the exponent a_3 are used to get an accurate representation of the iron losses at large flux densities by introducing a higher power of B. Thus, they are called high order loss factors. Further, a_3 is depending on the lamination thickness. The excess loss term C_{exc} is negligible compared to the other terms in this model and thus not regarded in (10) [24].
It should be mentioned that the history of the flux density waveform is not taken into account in the discussed Steinmetz equation models and in the loss separation models. But the described hysteresis models in the next section do this.

2.3 Hysteresis models

Mathematical hysteresis models simulate the used BH-hysteresis loop due to the applied flux density in electrical steel sheets. Since the shape and inner area of the BH-hysteresis loop is proportional to the iron losses, they can be applied to determine losses in electrical machines e.g. in FEM simulations. Hysteresis models require more measurement and material data of the used electrical steel sheets but also give better results in terms of accuracy and allow more complex simulations compared to the simpler Steinmetz models.
The most wide spread hysteresis models are the Preisach model [25,26] and Jiles/Atherton model [27], and they are still the base for further mathematical hysteresis models [28]. More information and a comparison between these two is presented in [29,30]. Since a detailed description of these models is beyond the scope of this paper, the reader is referred to relevant literature [26].
Some applicable improved and modified hysteresis models are amongst others the dynamic Preisach model, the Magnetodynamic Viscosity Based model, the Loss Surface model, the Friction Like Hysteresis model and the Energy Based Hysteresis model.
The dynamic Preisach model extends the classical Preisach model by introducing a rate dependent factor for each elementary rectangular loop of the hysteresis model [26,31,32]. It takes the delay time of the induction $B(t)$ behind the magnetic field $H(t)$ into account. Thus, it is possible to regard the enlargement of the hysteresis loop with increasing frequency.
The Magnetodynamic Viscosity based model [33] is similar and also based on a static (rate-independent) Preisach hysteresis model. But it uses a viscous type differential equation for describing the delay time between the induction $B(t)$ and the magnetic field $H(t)$. This differential equation determines the shape of the dynamic part of the loop and the dynamics of the model to take the excess losses into account.

2.4 Iron loss models in FEM software

Next to the standard loss separation model described in (7), most commercial FEM software packages offer in addition different more advanced models to determine iron losses from

electro-magnetic simulations. The software JMAG[1] uses a frequency separation approach to determine iron losses from the electro-magnetic simulation results (post processing) [34]. The eddy current losses are determined by

$$p_{\mathrm{ec}} = \sum_{k=1}^{n} \left[\sum_{l=1}^{N} b(|B_l|, f_l) f_l^2 \right] \tag{11}$$

where n is the number of elements, B_l the magnetic flux density at the frequency order l after a Fourier transformation, and $b(|B_l|, f_l)$ is determined by the frequency separation method [34]. To compute the hysteresis losses from a time series data of magnetic flux density, the number and size of hysteresis loops can be obtained. The hysteresis losses are determined by

$$p_{\mathrm{hyst}} = \sum_{k=1}^{n} \left[f \sum_{j=1}^{nloop} a(|B_j|) \right] \tag{12}$$

where B_j is the amplitude of the jth hysteresis loop, $nloop$ the number of loops, f the basic frequency and $a(|B_j|)$ is the coefficient of magnetic flux density which is determined from the frequency separation method

$$\frac{p_{\mathrm{Fe}}}{f} = a(B) + b(B,f) f \tag{13}$$

A dynamic and scalar post-processing hysteresis model, the Loss Surface model, is presented in [35] and implemented in the FEM software Flux[2]. The magnetic field H is determined as a characteristic surface function

$$S = H\left(B, \frac{\mathrm{d}B}{\mathrm{d}t}\right) = H_{\mathrm{stat}}(B) + H_{\mathrm{dyn}}\left(B, \frac{\mathrm{d}B}{\mathrm{d}t}\right) \tag{14}$$

separated into a static and a dynamic part. B is the magnetic flux density and dB/dt its rate of change. The model connects the magnetic field H on the sheet surface with the flux density B in the thickness of the sheet. The static part is modeled by the classical (static) Preisach model (rate-independent), which is determined by measurements of the major loop and first order reversal curves. The dynamic part is modeled by two linear analytical equations describing the low and high values of the flux density derivatives after subtracting H_{stat}.

Another implementation of hysteresis modeling in FEM software which focuses on a simple material data input approach is presented in [36] and implemented in the FEM software Opera[3] [37]. Here, the given non-linear BH-curve is used directly in the electro-magnetic FEM calculations to determine the magnetic field and flux distribution as well as the hysteresis and eddy current losses. In this process, also the history of the magnetization in each element is taken into account.

Finally, a possible implementation of the dynamic Preisach model into FEM software for iron loss determination in electrical machines is presented in [38, 39].

[1] JMAG is a registered trademark of the JSOL Corporation, Japan

[2] Flux is a registered trademark of the CEDRAT Group, France.

[3] Opera is the software package from Cobham Technical Services, UK

3 A Loss Separation Approach to Determine Iron Losses in Induction Machines

In electrical machines, the complex geometry and the combined use of different materials complicates the subdivision of the total losses into well defined categories. However, existing international standards have been developed to define the different loss components. For small to medium sized industrial induction machines, the ruling ones are IEC 60034-2-1 and IEEE-112. A comparative study of these two standards is reported in [40]. This section presents results from measurements of iron losses on a small three-phase induction machine, rated 11 kW, used for pump applications. In the following, the iron losses are defined according to IEC-60034-2-1 [41].

3.1 Distribution of losses at rated power

At rated output power, the total losses in the studied machine can be subdivided into different components, according to Figure 2. As expected for a small induction machine, most of the losses occur in the stator winding. However, for this machine, the second largest component is the iron losses. These losses are defined indirectly from a set of measurements performed under no-load conditions, referred to as a no-load test.

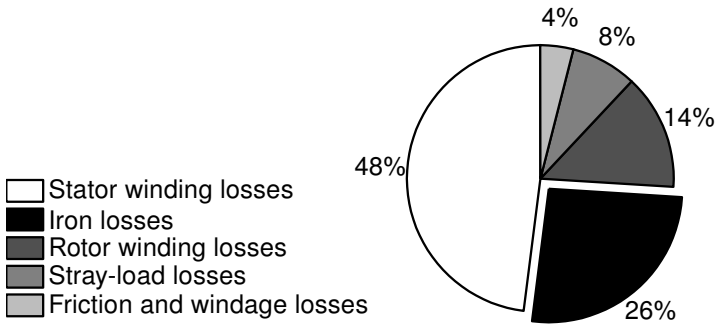

Figure 2: Distribution of the total losses at rated power for the studied 11 kW induction machine.

3.2 No-load test

In order to stabilize the no-load losses, the machine is operated at rated voltage and frequency until thermal equilibrium is reached. That is, according to the standard, when the no-load input power varies by 3 % or less, when measured at two successive 30 minutes intervals. Secondly, measurements are performed for a minimum value of seven different voltage levels, including rated voltage. The voltage being distributed between 20 % and 125 % of rated voltage. Quantities to be measured are; three-phase average stator current, average stator voltage, and input power. In order to minimize the temperature variations during the readings, the measurements shall be taken in descending order of voltage, as quickly as possible. Finally, after the lowest voltage readings, the stator winding resistance is measured.

As the mechanical output power is zero, the measured input power equals the total losses in the machine. Figure 3 shows the total no-load losses P_0, and the stator winding losses P_s, in the investigated induction machine as a function of the terminal voltage. Here, the stator winding losses are determined from the measured average line current and the measured winding resistance. At no-load, the studied induction machine is designed to operate close to or within the saturated region of the electrical steel. This, however, is common practice in machine design reducing the cost and the weight of machine. As a result, the no-load losses increase rapidly when the voltage exceeds the rating.

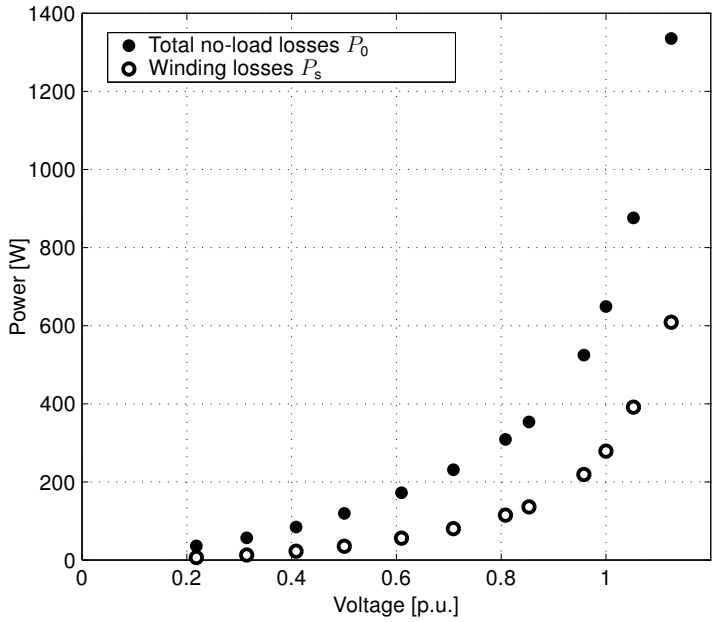

Figure 3: Measured no-load losses at rated frequency as a function of voltage.

3.3 Segregation of no-load losses

The total losses in the machine consists of stator winding losses (also called stator copper losses or Joule losses), iron losses, P_{Fe}, and friction and windage losses, P_{fw}. The standard defines a separation approach for the determination of the iron losses. Subtracting the winding losses from the total losses gives the so called "constant losses", according to Equation 15. These losses, i.e. the sum of the iron losses and the friction and windage losses, are shown as a function of the voltage squared in Figure 4a. Therefore, a linear behavior is obtained within the region where magnetic saturation is not present. For the points not affected by saturation, a straight line is extrapolated to zero voltage, the intercept with the zero voltage axis defines the friction and windage losses.

$$P_{\text{c}} = P_0 - P_{\text{s}} = P_{\text{Fe}} + P_{\text{fw}}. \tag{15}$$

The iron losses are obtained by subtracting the friction and windage losses from the constant losses. According to the standard, a curve defining the iron losses as a function of the voltage shall be developed as shown in Figure 4b. In the present IEC-standard, the iron losses are considered to be load dependent, taking the resistive voltage drop over the stator winding into account. In other words; an increased load results in increased current, hence,

the voltage drop over the stator winding increases, reducing the magnetizing voltage. As a result, the iron losses are reduced. However, this effect is mostly visible on small machines having a large stator resistance.

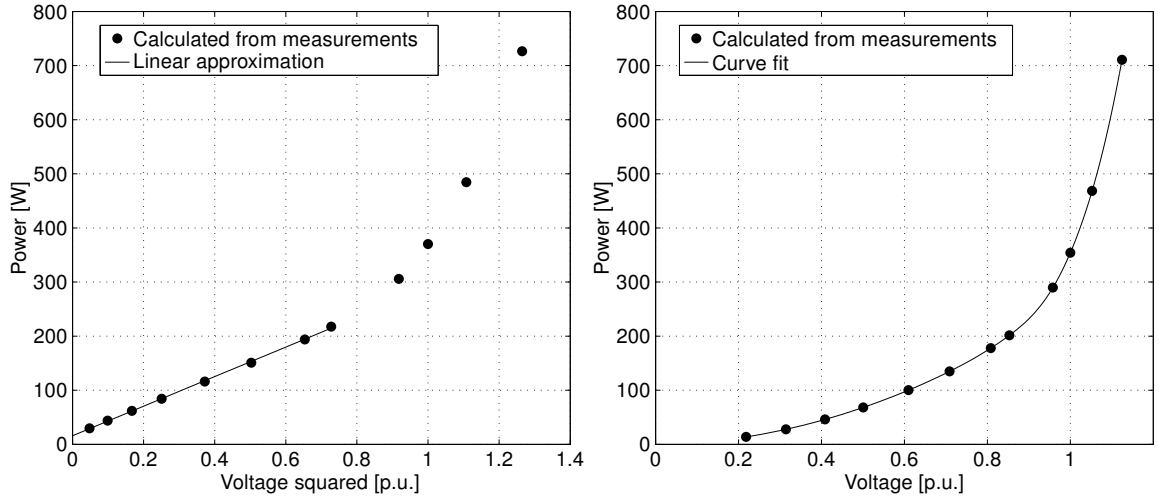

(a) Constant losses, P_c, as a function of voltage squared.

(b) Iron losses, P_{Fe} as a function of voltage.

Figure 4: Determination of friction and windage losses (a) and iron losses (b) from measurements.

3.4 Issues related to the loss separation approach

In the loss separation approach described above, the stator winding resistance is a crucial factor for an accurate determination of the iron losses. According to the standard used, this resistance is measured at the end of the no-load test. However, depending on the duration of the test, the winding resistance may vary between the different operating points. A better result would be obtained if the winding resistance was measured directly on-line for each operating point. Such a monitoring technique is presented in [42].

During the no-load test, it is obvious that the machine must operate without load, i.e. the rotor current being zero. However, due to friction losses in the bearings and windage losses along the rotor surface, the machine is loaded to some extent, introducing additional losses in the rotor circuit. This effect is usually small but the iron losses calculated from the no-load test still depends upon the friction and windage losses. This effect can be reduced by using high efficient bearings, resulting in a more accurate determination of the iron losses.

In an induction machine, parasitic effects such as airgap space harmonics created by the stator and rotor slotting give rise to additional losses, referred to as stray losses. When the machine is loaded, the standard defines these losses as stray-load losses. At no-load, however, the definition of the iron losses includes the stray no-load losses.

The existing standard procedures for measuring iron losses in electrical machines are adapted for a simplified and standardized testing in industry. The iron losses obtained

for such a test include several other sources of losses. As a result, the losses calculated by the use of traditional iron loss modeling will most likely seem to be underestimated.

4 Thermal Measurements to Investigate Iron Losses

In this method, first an accurate lumped parameter (LP) thermal model of an electrical machine is derived. Then, iron losses are calculated based on the derived thermal model and temperature measurements in the steady state.

4.1 Lumped parameter thermal model of a permanent-magnet assisted synchronous reluctance machine (PMaSRM)

LP thermal analysis and numerical methods are the major approaches used to model thermal effects in electric machinery [43]. The LP model represents a simplification, where spatially distributed fields are approximated as a number of single scalars. Thereby, a thermal analysis can be carried out, providing fast results with reasonable accuracy provided that the LP network is chosen with care.
Using LP thermal models of different parts of the PMaSRM described here, the LP thermal model of the machine is first implemented, and then solved using the software Portunus[4]. The complete thermal model, including the housing water jacket, is illustrated in Figure 5.

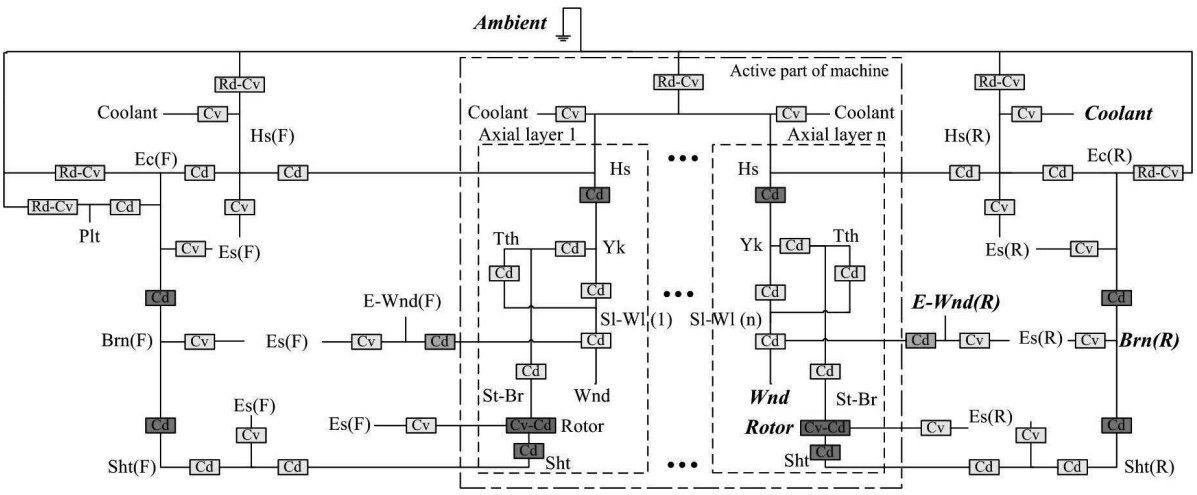

Figure 5: Complete LP thermal model of the PMaSRM. The abbreviations used are reported in Table 1. Loss sources are indicated as dots. The bold highlighted words also represent temperature sensor locations in the experimental setup.

To model the convective heat transfer from the stator housing to the coolant, the analytical formulations in [44, 45] and [46] are used. Also, the convective heat transfers from the end winding, shaft, and rotor to the end space are modeled analytically [47]. The LP thermal model representing the winding inserted in the slot is described in details in [48] where the copper and impregnation filling the slot is divided into a number of concentric ellipses. Based on the proposed elliptical model, a multi-layer structure of the winding thermal model

[4]Portunus is a registered trademark of the CEDRAT Group, France.

Table 1: Abbreviations used in Figure 5.

(F)	Front	Hs	Housing
(R)	Rear	Plt	Plate
Cd	Conduction	Sht	Shaft
Cv	Convection	Sl-Wl	Slot wall
Rd	Radiation	St-Br	Stator bore
Brn	Bearing	Yk	Stator yoke
Ec	End cap	Tth	Stator tooth
Es	End space	Wnd	Winding
E-Wnd	End winding		

is developed. For the rotor, it is assumed that surfaces normal to the radial direction are isothermals. Such an approximate “radial geometry" and corresponding LP thermal model are illustrated in [49]. The LP thermal models of the remaining parts of the PMaSRM can be found in [50–54].
In addition to the thermal resistances that can be calculated using analytical and numerical methods, there are a few thermal resistances that are difficult to estimate without experimental data available for model calibration. These resistances represent the contact resistance between the stator back and stator housing and the contact resistance between the rotor yoke and the shaft. The exact values of these thermal resistances depend on several factors, e.g. the manufacturing process, the size of machine and the used materials. Here, these resistances are first pre-estimated according to [55] and then calibrated using data from experimental tests.

4.2 Experimental setup

To obtain a good estimation of the produced iron losses and to calibrate the derived thermal model, temperatures of the stator, winding, coolant, and rotor should be monitored accurately. In this regard, twelve two-wire PT100 resistance temperature detectors (RTDs) are placed inside the winding and stator, and 3 RTDs are located in the rotor body. Also, two four-wire RTDs are used to measure temperatures of the inlet and outlet coolant.
The temperature sensors mounted in the rotor are connected to the measurement setup using a slip-ring unit mounted on the rotor shaft. The experimental setup is shown in Figure 6.

4.3 Comparison between the FEM and experimental results

The FEM software JMAG is used to compute the iron losses. Figure 7 shows the resulting iron loss density distribution in the stator and the rotor laminations for two operating points. In Figure 7a), the PMaSRM operates at rated speed (1500 rpm) and an average torque of 108 Nm and in Figure 7b), the PMaSRM rotates in the field weakening range (3000 rpm and 72 Nm). The used steel laminations are M250-35A.
A comparison between the calculated iron losses from FEM, as described above, and the calculated iron losses from the temperature measurements and the developed thermal model shows that the FEM results underestimate the produced iron losses in the studied

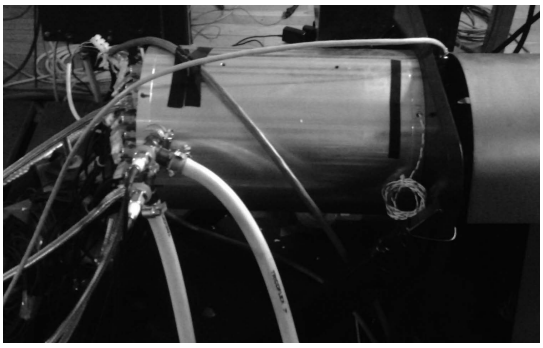

Figure 6: Experimental setup. The front hoses carry inlet and outlet water for the water jacket.

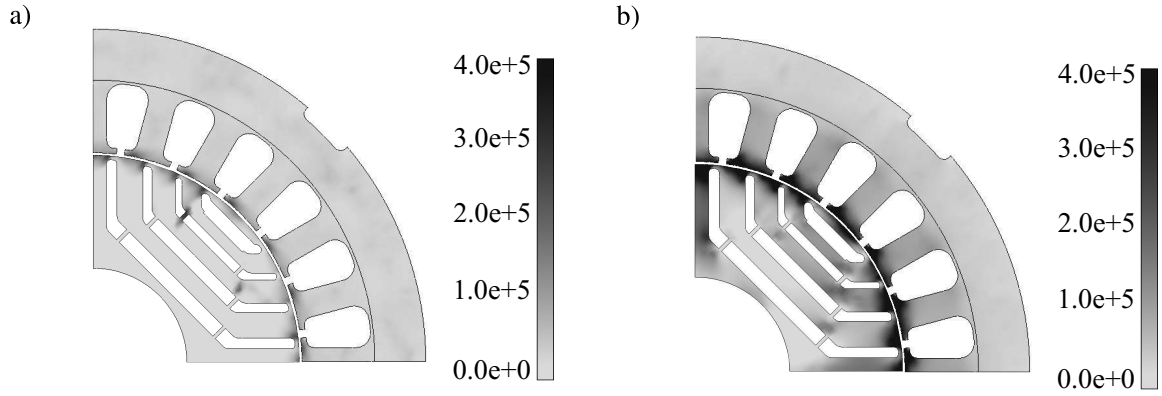

Figure 7: Resulting iron loss density distributions (W/m^3): a) 1500 rpm, 108 Nm; b) 3000 rpm, 72 Nm.

PMaSRM by up to 60 %. Using the 2D FEM computed iron losses as an input to the LP thermal model yielded in a temperature deviation between the LP model and the corresponding experimental results of 3 °C to 6 °C. The main reason for this deviation between the experimental and simulation results can be attributed to the influence of the manufacturing process on the produced iron losses and the accuracy of the adopted iron loss models.

5 Magnetic Material Characterization to Determine Iron Losses

Determining iron losses directly from electro-magnetic measurements is typically carried out for whole cores of small electrical machines and parts of larger machines. It is possible to analyze different parts separately, e.g. the stator and the rotor core or the stator teeth and stator yoke. The Epstein frame is normally used for testing the magnetic properties of laminated materials of a fixed size and the preferred choice for comparable measurements [56]. However, the preferred test for solid or small and special shaped materials uses sample parts machined into ring shape specimens, following the testing method described in IEC 60404-6 [57]. The rings are wound with a primary winding for the excitation of the core and a secondary winding for voltage measurements. The primary winding is supplied by either a sinusoidal current or a sinusoidal voltage and the flux in the ring core is obtained by

Figure 8: Wound stator ring cores for magnetic measurements.

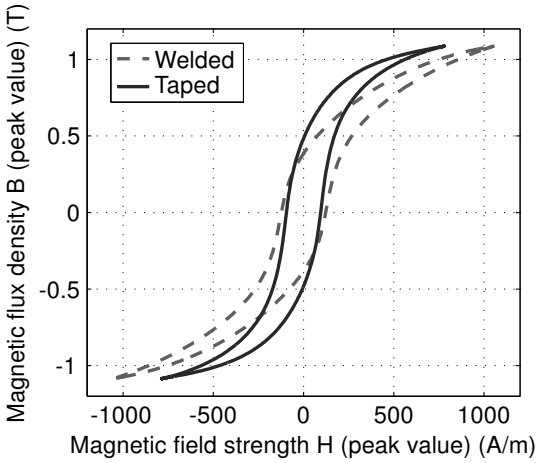

(a) BHmeasurement curves for a peak flux density of 1.1 T

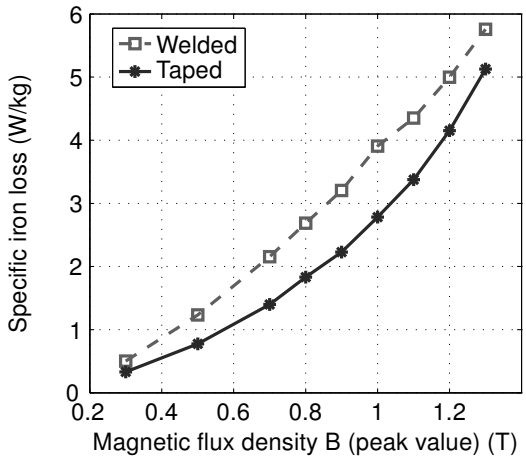

(b) Specific iron losses over the flux density

Figure 9: Measurement results of the welded and taped ring cores at 50 Hz.

integration of the voltage across the secondary winding. In the used setup a National Instruments CompactRIO system is used for the control and acquiring measurement results. The iron losses in the ring cores are determined by a Yokogawa WT3000 power meter. This test method is applied in an industrial project for small slot-less permanent magnet synchronous machine stator cores and passive parts of a large synchronous generator in the megawatt range, as described in the following.

5.1 Iron loss characterization of small permanent magnet machines

The study of the small slot-less permanent magnet synchronous machine stator cores focuses on the influence of the welding process during manufacturing. The cores are made from low-loss and thin electrical steel sheets produced by Cogent Surahammars Bruk AB (NO20). Each core is 64.5 mm long and has an outer and inner diameter of 31 mm and 23.2 mm, respectively. They are investigated before and after the welding process. The cores from before the welding process are wound and tightly pressed together by insulation tape. Four of the cores are shown in Figure 8. The flux density and magnetic field strengths measurement results for the welded and taped ring cores at 50 Hz are shown in Figure 9a. The increase of iron losses due to the welding process for different flux density peak values at 50 Hz is shown in Figure 9b.

It can be seen that the welding process during manufacturing of the stator ring core deteriorates the magnetic properties of the material significantly. The shape of the BH-curve is changing and the specific iron losses are increased for the welded cores. Further results will be published at the International Conference on Electrical Machines 2012 in Marseille.

5.2 Magnetic characterization of solid materials

Inactive parts of a large electrical machine (synchronous generator) are investigated in a similar way as the ring core test in order to determine the hysteresis loop (for hysteresis losses) and conductivity (for eddy current losses).
The tested solid material is a construction steel used for supporting the stator stacking (end rings of the investigated synchronous machine). The position of the end ring in the machine is shown in Figure 10. Even if the material is not used in the main flux path of the

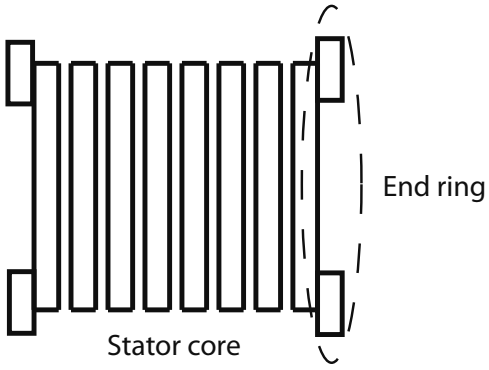

Figure 10: Location of the end rings at the stator core made of lamination packages and separated by cooling ducts.

machine, it is subject to a time varying magnetic field caused by leakage flux in the end region. Therefore, knowing its magnetic characteristics is important when trying to chase down the unaccounted losses measured in real machines.
Figure 11 shows the measured BH-curves for the tested material at different excitation levels with sinusoidal current supply. Figure 11a represents the results obtained at a frequency of 0.1 Hz, i.e. DC and Figure 11b shows the results measured at a frequency of 50 Hz. Already at 50 Hz, the eddy currents in the material are pronounced and its' effect is to counteract the excitation field which leads to an increased magnetizing field to reach a given level of flux. This in turn, forces the hysteresis curve to take the elliptical form as shown in Figure 11b.
Loss measurements at 50 Hz are shown in Figure 12. The flux density was varied from 0.2 T to 1.45 T and the active power was measured. The iron losses are proportional to the square of the flux density. At 1.45 T they reach 85 W/kg. As the tested material is solid, the eddy current losses are dominant.

5.3 Measurements of stator iron loss - core flux test

This test reveals any hot spots in the stator core of large electrical machines (i.e. MW range) after manufacturing and determines the iron losses in the yoke with a flux in the peripheral direction. Iron loss in the teeth is omitted as the flux path is in the yoke only.

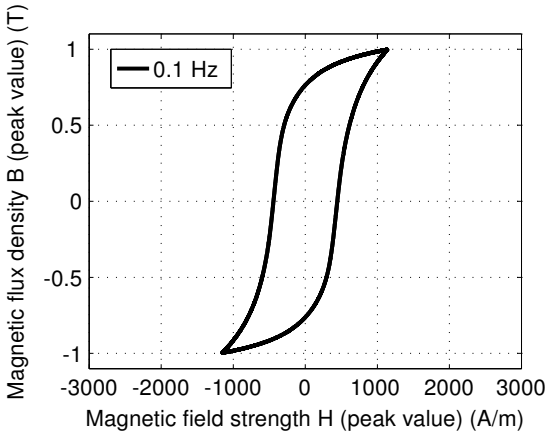

(a) BH-curve for the stator end ring at 0.1 Hz and varying excitation field.

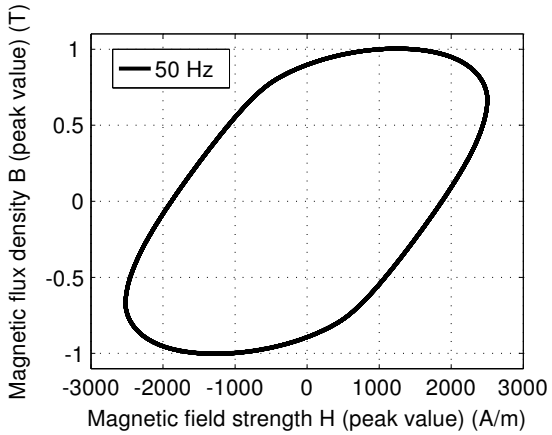

(b) BH-curve for the stator end ring at 50 Hz and varying excitation field.

Figure 11: BH-curves for the solid test sample representing the stator end ring.

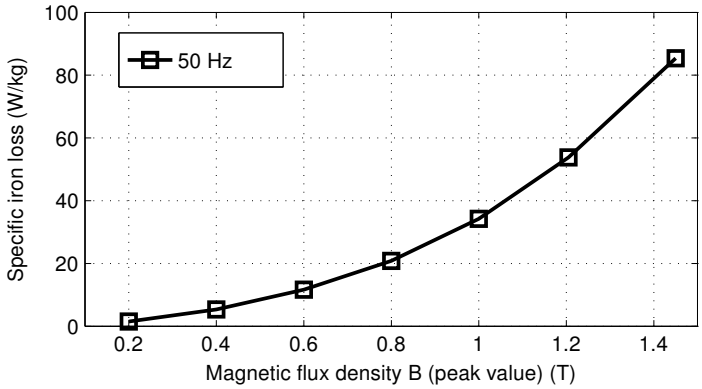

Figure 12: Measured iron loss at different flux densities.

The test is described in detail in [58]. It is performed before the stator is wound. A primary loop, consisting of a few turns is wound around the stator back and a secondary loop or measuring loop consisting of one or a few turns is also wound around the stator back. A current in the primary loop excites the stator core and the flux is calculated from the measured voltage in the secondary loop. The secondary voltage and primary current are used to calculate the power loss due to iron loss.

The core is then analyzed with a thermal camera to locate hot spots in the core surface. The hot spots are positions where excessive loss is produced, which is reflected in the temperature. The standard defines a hot spot as a point where the temperature exceeds 5 °C from the average surface temperature. A found hot spot is an indication that there is electrical contact between two (or several) stator laminations which has created a closed path for eddy currents. The increased iron losses associated to a hot spot may not be significant at a global level but locally hot spots may have disastrous effects, therefore, a local investigation is done using infra-red camera pictures. Figure 13a shows a thermal image of a stator during a core flux test. The temperature along the line Li1 is shown in Figure 13b. The results from this particular test show that no hot spots were found.

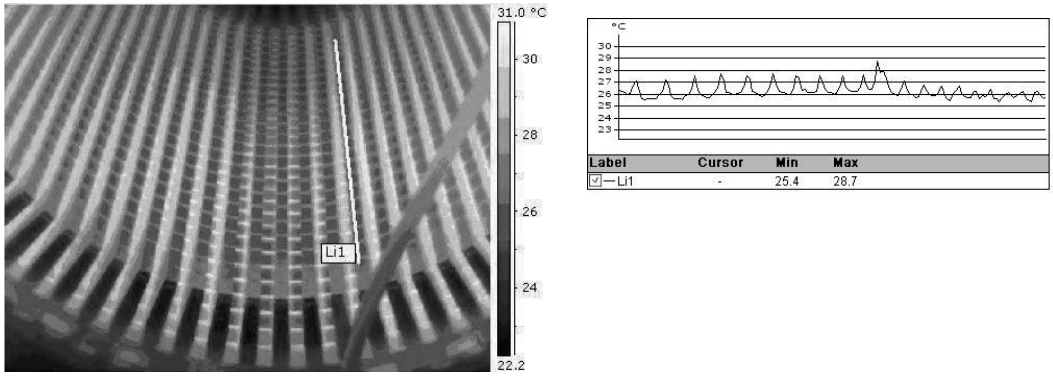

(a) Thermal image of a stator during core-flux test. (b) Temperature along line Li1 shown in 13a

Figure 13: Results from a core-flux test on a healthy stator.

6 Conclusion

Nowadays, machine designers and system engineers have the possibility to choose from a wide range of more or less complex iron loss simulation models for electrical machines. Several often used models were presented and described in more detail in this paper to give the reader a more comprehensive understanding and help choosing a suitable model. Different measurement methods used in ongoing research projects were described, illustrating advantages and disadvantages that can be expected from these methods.
The standardized procedures for measuring iron losses in electrical machines are adapted for a simplified testing in industry. These standards are important for comparability and repeatability of test results. However, it is shown that the iron losses obtained from a standard induction machine test using the loss separation approach also include other sources of losses. The same yields for the approaches based on direct temperature measurements. These are independent of uncertain parameters, e.g. the magnetization curve and frequency characteristics of the used materials. However, subtracting different loss sources in electrical machines is still a challenging research area for these methods. On the other hand, methods to determine iron losses in electrical machines by magnetic property measurements, i.e. measuring the magnetic field and flux density in different parts of a machine, can give accurate results locally. The challenge in this approach is to investigate and apply the correct flux density distributions in the studied local parts of the machine.
One of the major problems is still the discrepancy between simulations and measurements of iron losses due to the influencing factors from the manufacturing process, i.e. cutting and punching as well as welding. The simulation models underestimate in general the iron losses in electrical machines. However, one solution might be to combine numerical simulation results of field and flux density distributions with loss measurement results of local geometry parts. In this way more accurate results could be achieved.

Acknowledgment

The authors would like to thank the Swedish Center of Excellence in Electrical Power Engineering (EKC2) for financial support as well as the companies Bevi AB, ABB Motors, ABB Machines, Atlas Copco Tools AB, and Motor Design Ltd for the collaboration and support in the presented projects.

References

[1] A. Schoppa, J. Schneider, and C. D. Wuppermann, “Influence of the manufacturing process on the magnetic properties of non-oriented electrical steels,” *Journal of Magnetism and Magnetic Materials*, vol. 215, pp. 74–78, 2000.

[2] W. Arshad, T. Ryckebusch, F. Magnussen, H. Lendenmann, B. Eriksson, J. Soulard, and B. Malmros, “Incorporating lamination processing and component manufacturing in electrical machine design tools,” in *Industry Applications Conference, 2007. 42nd IAS Annual Meeting. Conference Records*, 2007, pp. 94–102.

[3] A. Schoppa, J. Schneider, and J. O. Roth, “Influence of the cutting process on the magnetic properties of non-oriented electrical steels,” *Journal of Magnetism and Magnetic Materials*, vol. 215-216, pp. 100–102, Jun. 2000.

[4] R. Rygal, A. J. Moses, N. Derebasi, J. Schneider, and A. Schoppa, “Influence of cutting stress on magnetic field and flux density distribution in non-oriented electrical steels,” *Journal of Magnetism and Magnetic Materials*, vol. 215-216, pp. 687–689, Jun. 2000.

[5] A. Schoppa, J. Schneider, C. D. Wuppermann, and T. Bakon, “Influence of welding and sticking of laminations on the magnetic properties of non-oriented electrical steels,” *Journal of Magnetism and Magnetic Materials*, vol. 254, pp. 367–369, 2003.

[6] A. Krings and J. Soulard, “Overview and comparison of iron loss models for electrical machines,” *Journal of Electrical Engineering*, vol. 10, no. 3, pp. 162–169, 2010.

[7] C. Steinmetz, “On the law of hysteresis (originally published in 1892),” *Proceedings of the IEEE*, vol. 72, no. 2, pp. 197–221, 1984.

[8] J. Li, T. Abdallah, and C. Sullivan, “Improved calculation of core loss with nonsinusoidal waveforms,” in *Industry Applications Conference, 2001. Thirty-Sixth IAS Annual Meeting. Conference Records*, vol. 4, 2001, pp. 2203–2210.

[9] K. Venkatachalam, C. Sullivan, T. Abdallah, and H. Tacca, “Accurate prediction of ferrite core loss with nonsinusoidal waveforms using only steinmetz parameters,” in *IEEE Workshop on Computers in Power Electronics*, 2002, pp. 36–41.

[10] H. Jordan, “Die ferromagnetischen Konstanten für schwache Wechselfelder,” *Elektr. Nach. Techn.*, vol. 1, p. 8, 1924.

[11] R. Boll, *Weichmagnetische Werkstoffe*, 4th ed. Publicis Corporate Publishing, 1990.

[12] R. H. Pry and C. P. Bean, “Calculation of the energy loss in magnetic sheet materials using a domain model,” *Journal of Applied Physics*, vol. 29, no. 3, pp. 532–533, Mar. 1958.

[13] G. Bertotti, “Physical interpretation of eddy current losses in ferromagnetic materials. I. theoretical considerations,” *Journal of Applied Physics*, vol. 57, no. 6, pp. 2110–2117, Mar. 1985.

[14] F. Fiorillo and A. Novikov, “An improved approach to power losses in magnetic laminations under nonsinusoidal induction waveform,” *IEEE Transactions on Magnetics*, vol. 26, no. 5, pp. 2904–2910, 1990.

[15] G. Bertotti, G. Di Schino, A. Ferro Milone, and F. Fiorillo, “On the effect of grain size on magnetic losses of 3% non-oriented SiFe,” *Le Journal de Physique Colloques*, vol. 46, no. 6, p. 385, 1985.

[16] G. Bertotti, “General properties of power losses in soft ferromagnetic materials,” *IEEE Transactions on Magnetics*, vol. 24, no. 1, pp. 621–630, 1988.

[17] W. A. Pluta, “Some properties of factors of specific total loss components in electrical steel,” *IEEE Transactions on Magnetics*, vol. 46, no. 2, pp. 322–325, 2010.

[18] A. Moses, “Importance of rotational losses in rotating machines and transformers,” *Journal of Materials Engineering and Performance*, vol. 1, no. 2, pp. 235–244, Mar. 1992.

[19] K. Atallah and D. Howe, “Calculation of the rotational power loss in electrical steel laminations from measured h and b,” *IEEE Transactions on Magnetics*, vol. 29, no. 6, pp. 3547–3549, 1993.

[20] T. Kochmann, “Relationship between rotational and alternating losses in electrical steel sheets,” *Journal of Magnetism and Magnetic Materials*, vol. 160, pp. 145–146, 1996.

[21] J. Sievert, H. Ahlers, M. Birkfeld, B. Cornut, F. Fiorillo, K. A. Hempel, T. Kochmann, A. Kedous-Lebouc, T. Meydan, A. Moses, and A. M. Rietto, “European intercomparison of measurements of rotational power loss in electrical sheet steel,” *Journal of Magnetism and Magnetic Materials*, vol. 160, pp. 115–118, Jul. 1996.

[22] N. Stranges and R. Findlay, “Measurement of rotational iron losses in electrical sheet,” *IEEE Transactions on Magnetics*, vol. 36, no. 5, pp. 3457–3459, 2000.

[23] L. Michalowski and J. Schneider, *Magnettechnik - Grundlagen, Werkstoffe, Anwendungen*, 3rd ed. Vulkan-Verlag GmbH, 2006.

[24] S. Jacobs, D. Hectors, F. Henrotte, M. Hafner, M. H. Gracia, K. Hameyer, P. Goes, D. R. Romera, E. Attrazic, and S. Paolinelli, “Magnetic material optimization for hybrid vehicle PMSM drives,” in *EVS24 - International Battery, Hybrid and Fuel Cell Electric Vehicle Symposium*, Stavanger, Norway, 2009.

[25] F. Preisach, “Über die magnetische Nachwirkung,” *Zeitschrift für Physik A Hadrons and Nuclei*, vol. 94, no. 5, pp. 277–302, May 1935.

[26] I. D. Mayergoyz, *Mathematical Models of Hysteresis and their Applications*, 2nd ed. Academic Press, Aug. 2003.

[27] D. Jiles and D. Atherton, “Theory of ferromagnetic hysteresis,” *Journal of Magnetism and Magnetic Materials*, vol. 61, no. 1-2, pp. 48–60, Sep. 1986.

[28] L. Dupre, R. Van Keer, and J. Melkebeek, “An iron loss model for electrical machines using the Preisach theory,” *IEEE Transactions on Magnetics*, vol. 33, no. 5, pp. 4158–4160, 1997.

[29] D. Philips, L. Dupre, and J. Melkebeek, “Comparison of Jiles and Preisach hysteresis models in magnetodynamics,” *IEEE Transactions on Magnetics*, vol. 31, no. 6, pp. 3551–3553, 1995.

[30] A. Benabou, S. Clénet, and F. Piriou, “Comparison of Preisach and Jiles-Atherton models to take into account hysteresis phenomenon for finite element analysis,” *Journal of Magnetism and Magnetic Materials*, vol. 261, no. 1-2, pp. 139–160, Apr. 2003.

[31] G. Bertotti, “Dynamic generalization of the scalar Preisach model of hysteresis,” *IEEE Transactions on Magnetics*, vol. 28, no. 5, pp. 2599–2601, 1992.

[32] L. R. Dupre, R. V. Keer, and J. A. A. Melkebeek, “On a magnetodynamic model for the iron losses in non-oriented steel laminations,” *Journal of Physics D: Applied Physics*, vol. 29, no. 3, pp. 855–861, 1996.

[33] S. Zirka, Y. Moroz, P. Marketos, and A. Moses, “Viscosity-based magnetodynamic model of soft magnetic materials,” *IEEE Transactions on Magnetics*, vol. 42, no. 9, pp. 2121–2132, 2006.

[34] “JMAG version 10 - User’s manual solver,” JSOL Corporation, Tokyo/2-5-24, Harumi, Chuo-ku, Tokyo, 104-0053, Japan, 2010.

[35] T. Chevalier, A. Kedous-Lebouc, B. Cornut, and C. Cester, “A new dynamic hysteresis model for electrical steel sheet,” *Physica B: Condensed Matter*, vol. 275, no. 1-3, pp. 197–201, Jan. 2000.

[36] S. E. Zirka and Y. I. Moroz, “Hysteresis modeling based on transplantation,” *IEEE Transactions on Magnetics*, vol. 31, no. 6, pp. 3509–3511, Nov. 1995.

[37] A. Michaelides, J. Simkin, P. Kirby, and C. Riley, “Permanent magnet (de-) magnetization and soft iron hysteresis effects: A comparison of FE analysis techniques,” *COMPEL: The International Journal for Computation and Mathematics in Electrical and Electronic Engineering*, vol. 29, no. 4, pp. 1090–1096, Jul. 2010.

[38] L. Dupre, O. Bottauscio, M. Chiampi, M. Repetto, and J. Melkebeek, “Modeling of electromagnetic phenomena in soft magnetic materials under unidirectional time periodic flux excitations,” *IEEE Transactions on Magnetics*, vol. 35, no. 5, pp. 4171–4184, 1999.

[39] O. Bottauscio, M. Chiampi, L. Dupré, M. Repetto, M. V. Rauch, and J. Melkebeek, “Dynamic Preisach modeling of ferromagnetic laminations : a comparison of different finite element formulations,” *Le Journal de Physique IV*, vol. 08, no. PR2, p. 4 pages, 1998.

[40] W. Cao, “Comparison of ieee 112 and new iec standard 60034-2-1,” *IEEE Transactions on Energy Conversion*, vol. 24, no. 3, pp. 802 –808, sept. 2009.

[41] “Rotating electrical machines - part 2-1: Standard methods for determining losses and efficiency from tests (excluding machines for traction vehicles),” International Standard IEC 60034-2-1:2007.

[42] S.-B. Lee and T. Habetler, “An online stator winding resistance estimation technique for temperature monitoring of line-connected induction machines,” *IEEE Transactions on Industry Applications*, vol. 39, no. 3, pp. 685 – 694, may-june 2003.

[43] A. Boglietti, A. Cavagnino, D. Staton, M. Shanel, M. Mueller, and C. Mejuto, “Evolution and modern approaches for thermal analysis of electrical machines,” *IEEE Transactions on Industrial Electronics*, vol. 56, no. 3, pp. 871–882, Mar. 2009.

[44] A. F. Mills, *Basic Heat and Mass Transfer*, 2nd ed. New Jersey: Prentice-Halls, 1999.

[45] D. K. Edwards, V. E. Denny, and A. F. Mills, *Transfer Processes*, 2nd ed. Washington, D.C.: Hemisphere, 1979.

[46] V. Gnielinski, "New equation for heat and mass transfer in turbulent pipe and channel flow," *Int. Chemical Engineering*, no. 16, pp. 359–368, 1976.

[47] E. Schubert, "Heat transfer coefficients at end winding and bearing covers of enclosed asynchronous machines," *Elektrie*, vol. 22, Apr. 1968.

[48] S. Nategh, O. Wallmark, M. Leksell, and S. Zhao, "Thermal analysis of a PMaSRM using partial FEA and lumped parameter modeling," *IEEE Transactions on Energy Conversion*, accepted for publication.

[49] S. Nategh, O. Wallmark, and M. Leksell, "Thermal analysis of permanent-magnet synchronous reluctance machines," in *Proc. 14th European Conf. Power Electronics and Applications (EPE'11)*, 2011.

[50] J. Lindström, "Development of an experimental permanent-magnet motor drive," Licentiate Thesis, Chalmers Univ. Technol., Göteborg, Sweden, Apr. 1999.

[51] P. H. Mellor, D. Roberts, and D. R. Turner, "Lumped parameter thermal model for electrical machines of TEFC design," *Proc. Inst. Elect. Eng. B*, vol. 138, no. 5, pp. 205–218, Sep. 1991.

[52] P. H. Mellor, D. R. Turner, and D. Roberts, "Microprocessor based induction motor thermal protection," in *Proc. 2nd Int. Conf. Electric Machine Design and Applications*, 1985, pp. 16–20.

[53] G. Kylander, "Thermal modelling of small cage induction motors," Ph.D. Dissertation, Chalmers Univ. Technol., Göteborg, Sweden, 1995.

[54] J. Saari, "Thermal analysis of high-speed induction machines," Ph.D. Dissertation, Helsinki Univ. Technol., Helsinki, Finland, 1998.

[55] A. Boglietti, A. Cavagnino, and D. Staton, "Determination of critical parameters in electrical machine thermal models," *IEEE Transactions on Industry Applications*, vol. 44, no. 4, pp. 1150–1159, Jul./Aug. 2008.

[56] "Methods of measurement of the magnetic properties of electrical steel strip and sheet by means of an epstein frame." International Standard IEC 60404-2:1998+A1:2008.

[57] "Methods of measurement of the magnetic properties of magnetically soft metallic and powder materials at frequencies in the range 20Hz to 200kHz by the use of ring specimens," International Standard IEC 60404-6:2003.

[58] P. Hamer, "Acceptance testing of electric motors and generators," *IEEE Transactions on Industry Applications*, vol. 24, no. 6, pp. 1138 –1152, nov/dec 1988.